metals

MDPI

Article

Study in Wire Feedability-Related Properties of Al-5Mg Solid Wire Electrodes Bearing Zr for High-Speed Train

Bo Wang [1], Songbai Xue [1,*], Chaoli Ma [1], Jianxin Wang [2] and Zhongqiang Lin [3]

[1] College of Materials Science and Technology, Nanjing University of Aeronautics and Astronautics, Nanjing 210016, China; wangbo4175@126.com (B.W.); machaoli006@163.com (C.M.)
[2] Jiangsu Provincial Key Laboratory of Advanced Welding Technology, Jiangsu University of Science and Technology, Zhenjiang 212003, China; wangjx_just@126.com
[3] Zhejiang Yuguang Aluminum Material Co., Ltd., Jinhua 321200, China; linzhongqiang666@163.com
* Correspondence: xuesb@nuaa.edu.cn; Tel.: +86-025-8489-6070

Received: 24 September 2017; Accepted: 20 November 2017; Published: 23 November 2017

Abstract: This work offers an analysis of the wire feedability-related properties of Al-5Mg solid wire electrodes bearing Zr. Effects of Zr content on microstructures and mechanical properties of the Al-5Mg alloys were studied. Experimental results have demonstrated that α-Al dendrites of the as-cast Al-5Mg alloy are refined, and the tensile strength, microhardness and roughness of the 1.2 mm wire electrode are improved with an appropriate addition of Zr. In addition, the tensile strength and elongation of the welded joints welded using Al-5Mg wire electrodes bearing Zr reach the maximum value when 0.12% Zr is added into the wire alloy. However, when excess Zr is added, α-Al phases of the wire alloy and welded joint are coarsened, and the mechanical properties are deteriorated. Moreover, the structure and principle of a novel apparatus, which can enhance the feedability of the wire electrode, are introduced and the apparatus can achieve the rough and fine adjustments of cast and helix of the wire electrode.

Keywords: Al-5Mg wire electrode; Zr; wire feedability; microstructure; mechanical properties

1. Introduction

Aluminum and its alloys are widely used in aerospace, railway, shipbuilding, pressure vessels and other fields due to their high specific strength, good corrosion resistance, and so on [1,2]. Among these applications, 5XXX, 6XXX and 7XXX aluminum alloys are often applied to the manufacture of high-speed train car bodies [3–5], and lots of research on advanced welding techniques for welding aluminum car bodies have been carried out at home and abroad [6–8]. With the development of robot welding automation technologies, the gas metal arc welding (GMAW) method has drawn much attention. During the GMAW process, the internal and external quality of welding consumables affect the shaping and quality of a weld. However, compared with imported aluminum wire electrodes, it is considered that domestic ones used for automatic and semi-automatic GMAW still have many urgent problems to be solved. These problems are serious arc wander and frequent downtime due to wire feeding problems [9].

The issue of aluminum wire electrode feedability has been studied by several authors [10–12]. Padilla et al. [10] reported that a key factor in the performance of GMAW was the feedability of the welding wire through the wire liner, and for aluminum wire electrodes, fluctuations in the wire feed speed (WFS) of even 1% could result in irregular arc lengths, oscillatory voltage and current levels, and the degradation of the overall weld quality. In part, variations in the target WFS were caused by adverse conditions during welding. These included damaging effects such as the "stick-slip" motion of the welding wire, the premature wear of the contact tube and, in general, the movement of the

hose package during welding. Previous research has pointed out that, during an automatic GMAW process, considering only the characteristics of the aluminum wire electrode, the stability of arc is mainly determined by the diameter, stiffness (column strength and elongation), surface quality and the winding characteristics of the wire electrode [9,11–14]. The Al-5Mg wire electrode, which is based on Mg as the main alloying element, is a kind of general-purpose welding consumable for welding 5XXX, 6XXX and 7XXX alloys. Tang et al. [9] studied the effect of the column strength of the ER5356 wire electrode with a diameter of 1.2 mm on the wire feedability during welding. They found that the wire electrode with a high column strength (448 MPa) could offer very good rigidity and was easier to push through a GMAW torch. In addition, ER5356 wire electrode with higher column strength has also been proved to feed better and yield welds that are stronger and more ductile compared with ER4043 wire electrode [13,14]. However, there still exists a huge gap between imported Al-Mg wire electrodes and domestic ones in terms of chemical composition control, melt refining, wire drawing and surface finishing technologies.

The method of microalloying plays a vital role in improving the mechanical properties of the aluminum alloy. Researches [15–19] have revealed the influences of some modification elements such as Zr, Sc and Er on the microstructure and mechanical properties of the aluminum wires and/or the welded joints. Al-Zr alloys have already been used according to international standard IEC 62004 by a number of widely known companies, such as Lamifil (Hemiksem, Belgium), 3M (Minnesota Mining and Manufacturing; St. Paul, MN, USA), J-Power Systems (Hitachi; Ibaraki, Japan) and others during the development of a heat-resistant aluminum wire for overhead power transmission lines [15]. Chao et al. [16] studied the mechanical properties and electrical conductivities of aluminum conductive wires of Al-0.16Zr, Al-0.16Sc, Al-0.12Sc-0.04Zr (mass %) and pure Al (99.996%) with a diameter of 9.5 mm. They found that the separate addition of 0.16% Sc and 0.16% Zr to pure Al improved the ultimate tensile strength but reduced the electrical conductivity, and a similar trend was found in the Al-0.12Sc-0.04Zr alloy. As for Al-Mg alloy, Taendl et al. [20] also reported that a balanced addition of small amounts of Sc and Zr was considered as one of the most promising approaches to increasing the specific strength of Al-Mg alloys, while maintaining the beneficial materials properties. With regard to the microalloying of the Al-5Mg welding wire, Norman et al. [21] researched the influence of the Sc concentration in the fusion zone of GMAW welds of typical 7XXX aluminum aerospace alloys; they noted that the Sc-bearing welding wire greatly outperformed all the conditional commercial welding wires (ER5087, 5180 and 5039), both in terms of weld strength and ductility. Zhang et al. [19] indicated that the addition of Sc into the aluminum alloy could ostentatiously boost the strength of alloy, while the low cost element Er shared similar functions with Sc in the aluminum alloy, so they studied the microstructure characteristics of welded joints of 7A52 welded by fiber laser, and using Al-Mg-Mn welding wire and Al-Mg-Mn-Zr-Er welding wire, respectively. They found that a huge amount of fine equiaxed grains was formed in the weld zone of Zr and Er micro-alloying Al-Mg-Mn welding wire. Xu et al. [18] also investigated the influence of the combinative addition of Er and Zr on the microstructure and mechanical properties of the GTAW welded joints of 7A52. By comparing the reference [18,19], although the thicknesses of the aluminum alloy plates were different (4 mm and 20 mm, respectively) and the welding methods were different (GTAW and fiber laser welding, respectively), a significant grain refinement was found in the weld zone of the two welded joints due to the formation of fine Al_3Er, Al_3Zr and Al_3(Zr, Er).

The abovementioned investigations focused mainly on the influence of the separate addition of Zr or the combinative addition of Zr and Er (or Sc) on the microstructures and the mechanical properties of aluminum conductive wires (pure aluminum) or the welded joints of 7XXX alloy. However, very few studies have been focused on the influence of the separate addition of Zr used as microalloying element on the wire feedability related properties of the Al-5Mg wire electrode. Therefore, the microstructure and mechanical properties of the Al-5Mg wire alloys bearing different contents of Zr were investigated in this study. The produced wires with diameter of 1.2 mm were used to welding the 5083-H112 plate. The 5083 alloy was selected as the welding coupons according to the European Standard EN 14532-3:2004 [22] and according to the specifications of approval testing for Al-5Mg welding wire specified by the Deutsche Bahn (DB) and the American Bureau of Shipping

(ABS). The optimum Zr content in Al-5Mg wire alloy was obtained by the analysis of effects of Zr on the wire feedability-related properties of Al-5Mg-*x*Zr wire electrodes and mechanical properties of resulting welded joints. Furthermore, a novel adjustable apparatus to enhance the wire feedability of the wire electrode was also introduced and the principle, structure and application results of the apparatus were simply analyzed.

2. Materials and Methods

Wire alloy for experiments was prepared using pure aluminum (99.7% Al), magnesium ingot, metal additives (75% metal) of manganese, titanium and chromium. The trace element Zr was added in the form of Al-10Zr master alloy at 720–750 °C, and the melt was purged with hexachloroethane (C_2Cl_6) and pure argon. The chemical compositions of wire electrodes are listed in Table 1, and the composition was measured using a SPECTRO® MAXx04D spectrometer (SPECTRO Analytical Instruments GmbH, Kleve, Germany).

Table 1. Chemical compositions of wire electrodes (wt %).

No.	Material	Mg	Mn	Cr	Ti	Zr	Al
1#	Al-5Mg	4.93	0.124	0.06	0.08	0.0003	balance
2#	Al-5Mg-0.06Zr	5.03	0.122	0.06	0.08	0.058	balance
3#	Al-5Mg-0.12Zr	5.05	0.123	0.06	0.08	0.123	balance
4#	Al-5Mg-0.24Zr	4.98	0.121	0.06	0.08	0.236	balance
5#	Al-5Mg-0.5Zr	5.07	0.122	0.06	0.08	0.52	balance

The casting process was conducted using a continuous casting and direct water-cooling method. The produced cast rods with a diameter of approximately 8.0 mm subsequently underwent these procedures, which included annealing-rolling-annealing-drawing-shaving-cleaning, to prepare the 1.2 mm diameter wire electrodes. The base metal was 5083-H112 alloy with dimensions of 10 mm × 175 mm × 350 mm intended for GMAW. Prior to welding, the base material coupons were wire brushed and degreased with acetone. The welding process was carried out according to the standard developed by ABS: "ABS-2017: Rules for Materials and Welding-Part 2: Aluminum and Fiber Reinforced Plastics (FRP)". An AOTAI P-MIG 500 welder (Aotai Electric, Jinan, China) was employed to weld the AA5083 plate.

Tensile specimens were prepared from the 1.2 mm wire electrodes and from the welded coupons. Each wire electrode used for tensile test was 200 mm long and the gauge length was 100 mm. Full-size transverse tensile specimens were machined from the welded plates according to ASTM E8 so that the weld was centered in the gauge section (the gauge length was 100 mm), and the loading axis was normal to the welding direction. To avoid the effect of weld profile on the stress concentration during the tensile test, the weld reinforcement was grinded with a polisher (Fujian Hitachi Koki Co., Ltd., Fuzhou, China) prior to being tested. Tensile tests were performed respectively on a WDW-20E electronical universal testing machine and a WAW-300B hydraulic one (Zhejiang Jingyuan Mechanical Equipment Co., Ltd., Jinhua, China). The elongation of the wire electrode and the resulting welded joint was the ratio of the variation in the gauge length to the original gauge length value. The Vicker's hardness measurements were conducted with 1.0 mm spacing on the wire electrodes and the cross section of these welded joints using an HXS-1000A microhardness tester (Teshi Testing Technology (Shanghai) Co., Ltd., Shanghai, China), under a load of 2.94 N for 15 s. Microstructures of Al-5Mg-*x*Zr alloys and the resulting welds were characterized using a TV-400D optical microscopy (Shanghai Tuanjie Instrument Manufacturing Co., Ltd., Shanghai, China) and a ZEISS ΣIGMA field-emission scanning electron microscope coupled to an energy dispersion X-ray (FE-SEM/EDX; Carl Zeiss, Oberkochen, Germany).

3. Results and Discussion

3.1. Microstructures of As-Cast Al-5Mg-xZr Wire Alloys

Figures 1 and 2 show the optical microstructures and the scanning electron microscopy (SEM) microstructures of as-cast Al-5Mg-xZr wire alloys, respectively. As shown in Figures 1a and 2a, the alloy (no alloying Zr) was mainly composed of α-Al matrix, granule Mg_5Al_8 precipitated phase and a small amount of Mn- or Cr-bearing intermetallic compounds (IMCs). Most of Mg element was dissolved in the α-Al matrix. However, the α-Al grains, which occupied a large volume fraction in the microstructure, were coarse and unevenly distributed. When adding 0.06 wt % Zr into the as-cast alloy, α-Al dendrites were refined (Figure 1b). With the increase of Zr content, the refinement effect on α-Al dendrites was further enhanced. When the addition of Zr in the wire alloy was 0.12%, refined equiaxed α-Al dendrites were obtained, the size of which was the smallest (Figures 1c and 2b). However, with a further increase in Zr content (up to 0.24% Zr), the size of α-Al grains became large.

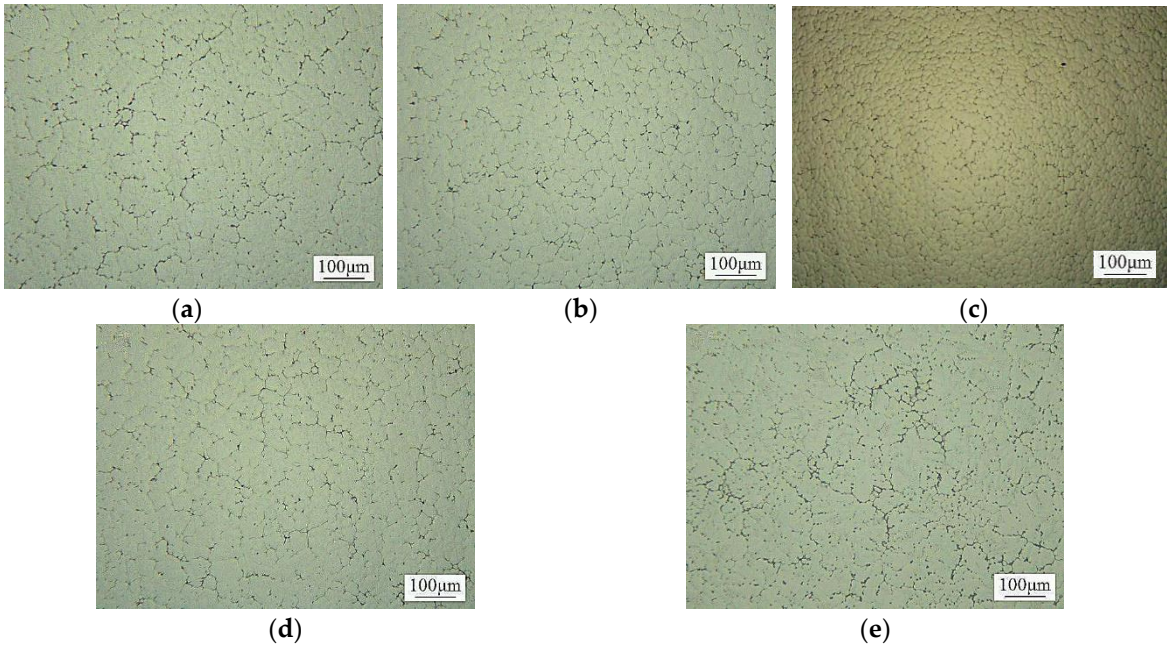

Figure 1. Optical microstructures of as-cast Al-5Mg-xZr alloys: (**a**) x = 0; (**b**) x = 0.06; (**c**) x = 0.12; (**d**) x = 0.24; (**e**) x = 0.5.

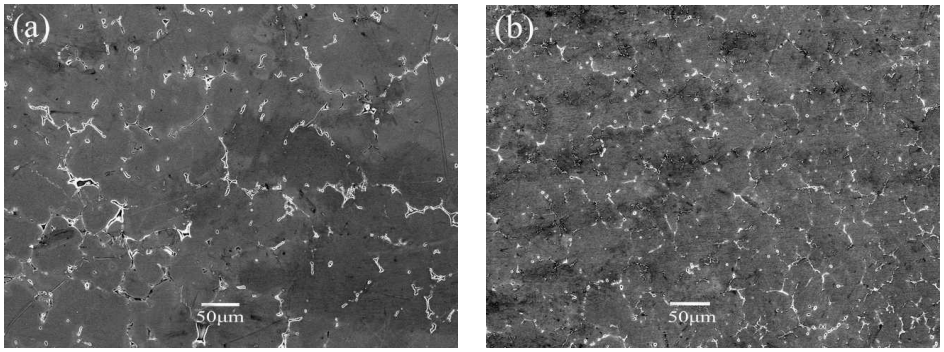

Figure 2. Scanning electron microscopy (SEM) microstructures of as-cast Al-5Mg-xZr alloys: (**a**) x = 0; (**b**) x = 0.12.

As shown in Figure 1e, when the content of Zr in the alloy reached 0.5%, α-Al dendrites in the matrix were obviously coarsened, and the microstructure uniformity of the as-cast alloy was seriously deteriorated. Figure 3 shows the SEM microstructure at high magnification of the as-cast Al-5Mg-0.5Zr alloy. Coarse lath-like IMCs were found on the surface of the α-Al phase. A further

EDS (Energy Dispersive Spectroscopy) analysis of the lath-like IMC (Point A; IMC: Intermetallic Compound) showed that the lath-like IMC consisted of element Al and Zr and the atomic ratio of Al to Zr was close to 3:1. Thus, the lath-like phase could be determined as the Al_3Zr phase.

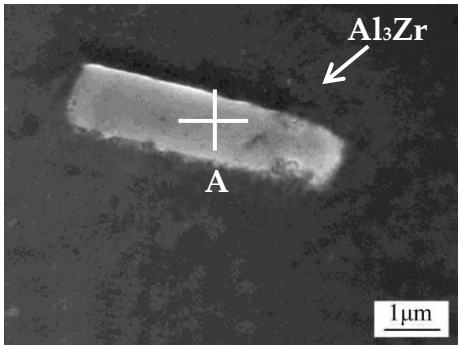

Figure 3. SEM image of the lath-like IMC (Intermetallic Compound) bearing Zr.

The refining effect of element Zr on α-Al dendrites in the wire alloy can be explained through the following analysis: when no Zr was added, Ti in the alloy chemically reacted with Al, producing fine Al_3Ti phases with uniform distribution. Al_3Ti phases were effective heterogeneous substrates for nucleation of α-Al dendrites and, hence, led to the refinement of α-Al phases. However, Ma et al. [23] had discovered that the refining effect of Ti addition alone on Al-Mg alloy was limited, and excessive Ti would result in the serious segregation of Ti in the alloy, which deteriorated the refining effect of Ti on α-Al dendrites. When adding a proper amount of Zr into the wire alloy (Figures 1b,c and 2b), finely dispersed Al_3Zr particles, which kept coherent with Al matrix, were produced from the peritectic reaction of Zr and Al [24]. According to the theory of heterogeneous nucleation, the combined effect of Al_3Zr particles and Al_3Ti phases greatly increased the amounts of heterogeneous substrates and then significantly enhanced the refining effect on the alloy. In addition, according to the Al-Zr binary phase diagram, the maximum solid solubility of Zr in Al was only 0.07%. Thus, during the solidification of liquid Al-5Mg-0.12Zr alloy, element Zr was enriched in front of the solid-liquid interface and led to constitutional supercooling, which promoted the necking of α-Al dendrites, increased the amounts of secondary dendrites and then refined α-Al grains of the wire alloy. However, when excess Zr was added, a large number of Al_3Zr IMCs would form in the alloy, which reduced the enrichment of Zr at the front of solid-liquid interface, resulting in the coarsening of the microstructure.

3.2. Mechanical Properties of 1.2 mm Al-5Mg-xZr Wire Electrodes

Figure 4a shows the tensile strength of Al-5Mg-xZr wire electrodes with a diameter of 1.2 mm. As can be seen, the tensile strength and elongation of Al-5Mg wire electrodes were both improved by adding trace Zr. These results show that when the content of Zr was 0.12%, the mechanical properties of the wire achieved the best, and the tensile strength and elongation were increased by 4.8% and 30.4%, respectively, compared with those of the Zr-free wire. Figure 5 shows the tensile curves of the Zr-free and Al-5Mg-0.12Zr wire electrode with the diameter of 1.2 mm. As can be seen from Figure 5, the tensile curves of the two wire electrodes showed typical yield behavior and the fracture mechanism of the two kinds of alloys was a ductile fracture due to significant plastic deformation. However, with a further addition of Zr, the tensile strength and elongation of the wire electrode declined. When the content of Zr was 0.5%, the mechanical properties of the wire electrode were even lower than those of the Zr-free wire.

Figure 6 shows the longitudinal-sectional metallographic structure of the 1.2 mm Al-5Mg-0.12Zr wire electrode. As can be seen from Figure 6, an obvious orientation was observed in the microstructure of the finished wire electrode, and the grains were refined evidently by wire drawing. Under the same process conditions (drawing and annealing), according to the hereditary microstructure, due to the refinement of the original as-cast structure of wire alloy by adding an

appropriate amount of Zr, the microstructure of the finished Al-5Mg-0.12Zr wire electrode was still better than that of others in the grain size. In addition, when annealed at 410 ± 10 °C, recrystallization accompanied with softening would occur in the semi-finished wire alloys with a deformed microstructure. Researchers have found that the addition of Zr and/or Sc elements could cause the resistance to recrystallization due to Zener pinning effect from secondary precipitates [15,16,25]. Therefore, it could be deduced that Al_3Zr phases, which were distributed dispersively in the matrix, inhibited the recrystallization of the annealed semi-finished wire alloys. According to the Hall–Petch formula, the refinement of the microstructure could improve the mechanical strength of the alloy. Crack initiation and propagation did not easily occur in the alloy with fine grain structure, thus the alloy showed high elongation. On the other hand, when excess Zr was added, a large number of lath-like IMCs appeared and the effect of grain refinement strengthening and the grain pinning effect on recrystallization was weakened, which resulted in the decline in the tensile strength and elongation of the finished wire electrode.

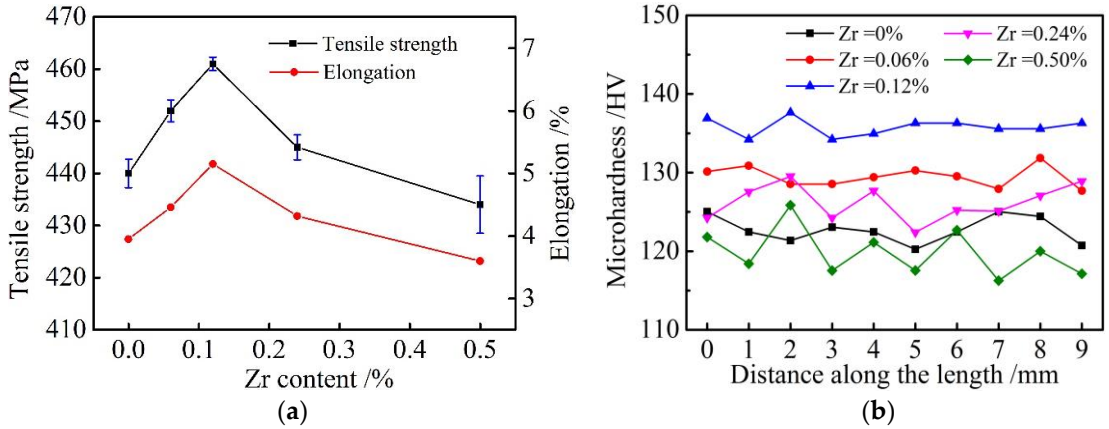

Figure 4. Mechanical properties of 1.2 mm Al-5Mg-*x*Zr wire electrodes: (**a**) tensile strength; (**b**) microhardness.

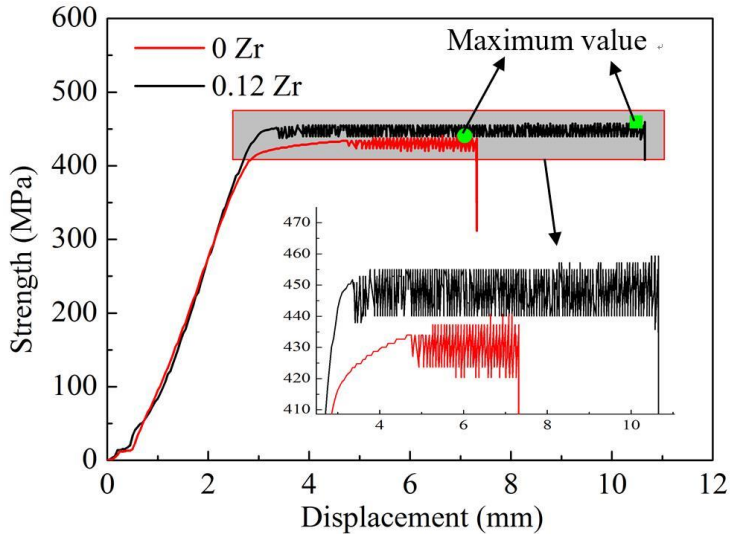

Figure 5. Tensile curves of 1.2 mm Al-5Mg and Al-5Mg-0.12Zr wire electrodes.

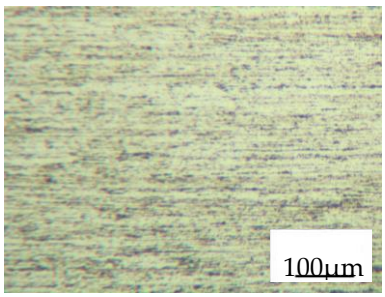

Figure 6. Longitudinal-sectional microstructure of the 1.2 mm Al-5Mg-0.12Zr wire electrode.

The microhardness results of 1.2 mm Al-5Mg-xZr wire electrodes are shown in Figure 4b. After adding an appropriate amount of Zr, the average hardness of the wire electrode increased, and the fluctuation value of hardness along its length was small. However, for the Zr-free wire electrode or the wire electrode with excess Zr addition, the average value of hardness was small and the fluctuation of hardness was large. The hardness evolution of Al-5Mg-xZr wire electrodes is mainly determined by the constituent of the alloy, morphology, size and distribution of α-Al phases, Mg_5Al_8 particles and so on. For Al-5Mg-xZr alloy, the finer the α-Al grain, the higher the hardness of the wire. According to the structure heredity of aluminum alloy, the as-cast Al-5Mg-0.12Zr alloy has fine equiaxed α-Al grains in its microstructure, thus its average hardness was the highest. In addition, the hardness of the alloy has a certain relationship with its surface roughness and the friction coefficient of the alloy is represented by:

$$\mu = \frac{\tau}{H} + \tan\theta + \mu_{\mathrm{p}} \quad (1)$$

where μ is the friction coefficient of the alloy, τ is the ultimate shear strength, H is the hardness, θ is the angle of friction surface, and μ_{p} is the component when the plow effect is considered. According to Equation (1), keeping other variables constant, the higher the H, the lower the μ. Therefore, the addition of Zr can not only refine the microstructure of the wire alloy, increase the tensile strength and hardness of the wire electrode, but also reduce the friction coefficient of wire surface, enhance the wire feedability of the wire electrode during the GMAW process.

3.3. Roughness of 1.2 mm Al-5Mg-xZr Wire Electrodes

The shaving process is extremely important in removing the oxide that forms on the surface of the wire alloys. Figure 7 shows the surface topographies of Al-5Mg-xZr (x = 0, 0.12, 0.5) wires, which were mechanical shaved with shaving dies made of synthetic diamond. As can be seen, the surface quality of the Zr-free wire was not high, and there was a small number of longitudinal scratches on the surface of the wire. According to the standard BS EN 14532-3 [22], longitudinal scratches can be acceptable, but could adversely affect the welding characteristics of the wire. The surface quality of Al-5Mg-0.12Zr wire was the best and the surface finish was smooth, uniform and free of scratches (Figure 7b). However, when the content of Zr was 0.5%, the dull matt surface of the wire was full of scratches and depressions, which was unacceptable according to BS EN 14532-3 [22].

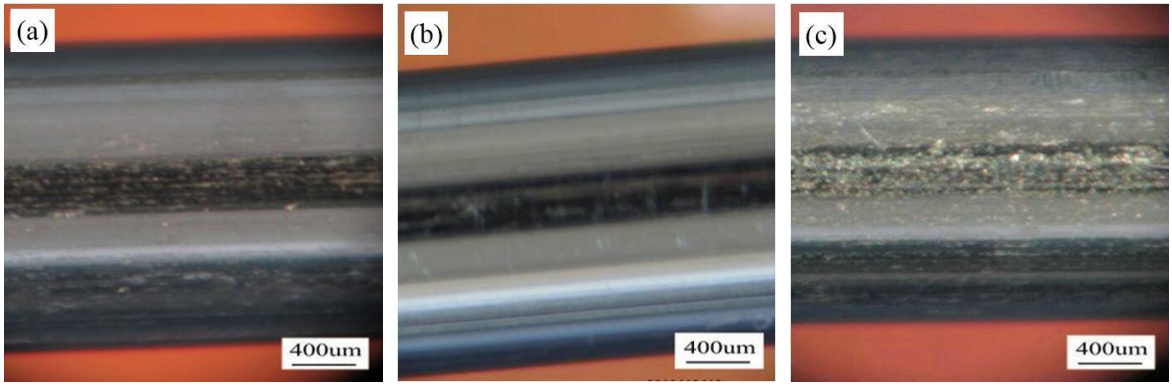

Figure 7. Roughness of 1.2 mm Al-5Mg-*x*Zr wire electrodes: (**a**) $x = 0$; (**b**) $x = 0.12$; (**c**) $x = 0.5$.

Abrasive wearing is the main wearing mechanism of the shaving die. During the shaving process, with the deformation of the Al matrix, most of IMCs embedded in the Al matrix of the wire were transferred into the Al chips or the surface of the shaved wire. With regard to the Al-5Mg-0.12Zr wire, because that fine α-Al dendrites of the wire alloy were evenly distributed and the fluctuation of wire hardness was very small, a large and uniform plastic deformation appeared in the Al matrix of the wire during the shaving process, which led to a relatively good surface quality of the wire. Whereas when 0.5% Zr was added, a large number of coarse IMCs in the microstructure of the wire were easy to slip toward the surrounding coarse Al matrix, some even were stripped from the Al matrix, leaving lots of irregularly distributed pits in various sizes on the surface of the wire. A small and uneven plastic deformation appeared in the Al matrix due to the coarse α-Al phases and IMCs, which easily caused stress concentration and resulted in crack initiation and propagation. In addition, the cutting edge of the die was under uneven stress and showed significant wear due to the strong friction between the shaving die and coarse IMCs. Cutting chips were easy to stick on the worn cutting edge of the shaving die, and thus produced many imperfections on the surface of the wire, deteriorating the surface quality of the wire.

3.4. Mechanical Properties of Welded Joints Welded Using 1.2 mm Al-5Mg-xZr Wires

Figures 8 and 9 shows the optical microstructures of different zones of welded joints of 5083 alloy welded using 1.2 mm Al-5Mg-*x*Zr wire electrodes. As shown in Figure 8a, a considerable number of black precipitated phases was homogeneously distributed along a certain direction, which indicated that the base metal was heavily rolled. As for the heat-affected zone (HAZ), its wide range was mainly composed of fibrous tissues, which were elongated along the rolling direction and were almost the same as those of base metal (BM) (Figure 8b). As can be seen from Figure 9a, the microstructure of the weld center mainly consisted of coarse α-Al phases and Mg_5Al_8 particles. Most of these particles were distributed in the grains, and others were precipitated in grain boundaries. When adding an appropriate amount of Zr, the microstructure of the weld center was refined (Figure 9b,c). The size of α-Al grains of the weld center reached the minimum value when 0.12% Zr was added. The refinement of the microstructure of the weld center was due to the large number of fine Al_3Zr, Al_3Ti and Al_3(Zr, Ti) particles [26–28], which formed during the solidification of welding pool and acted as substrates for heterogeneous nucleation of α-Al phases. Figure 10a also showed that the tensile strength of the welded joint welded using Al-5Mg-*x*Zr wire reached the maximum value of 312.6 MPa with the adding of 0.12% Zr. Figure 10b shows the microhardness distributions of the welded joints with Al-5Mg (Zr-free) and Al-5Mg-0.12Zr wire electrode, respectively. As shown in Figure 10b, the minimum hardness value was located in the weld zone (WZ), which indicated that the frail position of the joints was located at the HAZ. After adding 0.12% Zr, the minimum hardness of the WZ increased, and the average hardness of the WZ increased. The microhardness evolution of the WZ can be explained by the abovementioned observation and analysis of the microstructure in Figure 9.

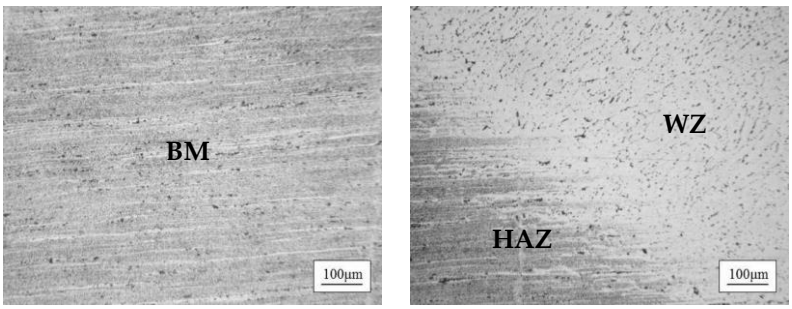

Figure 8. Optical microstructures of different zones of welded joints at low magnification that were welded using 1.2 mm Al-5Mg-0.12Zr wire electrodes: (**a**) BM (base metal); (**b**) HAZ (heat-affected zone) and WZ (weld zone).

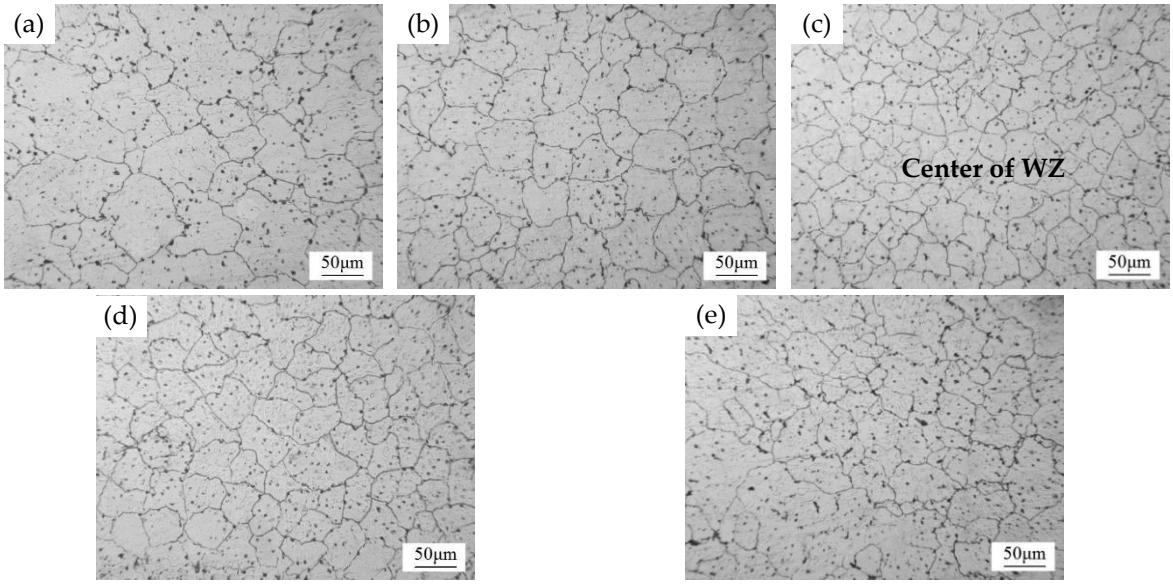

Figure 9. Optical microstructures of the weld center of welded joints at high magnification welded using 1.2 mm Al-5Mg-*x*Zr wire electrodes: (**a**) $x = 0$; (**b**) $x = 0.06$; (**c**) $x = 0.12$; (**d**) $x = 0.24$; (**e**) $x = 0.5$.

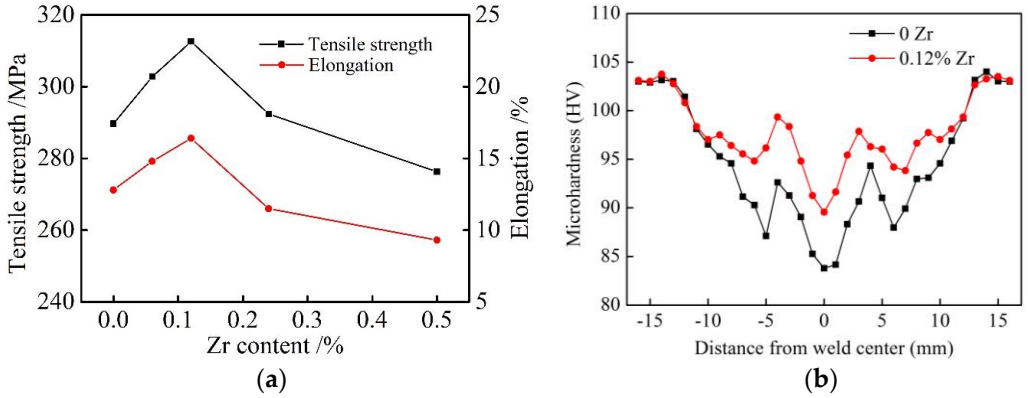

Figure 10. Mechanical properties of the welded joints with 1.2 mm Al-5Mg-*x*Zr wire electrodes: (**a**) tensile strength (fracture location: weld zone); (**b**) microhardness distribution across the welded joints.

3.5. Novel Apparatus for Adjusting Wire Feedability-Related Properties during Drawing Process

After further increasing the Zr content to 0.24% (Figure 9d), the α-Al grains of the weld center became coarse and were varied in size. Furthermore, when the Zr content was 0.5%, large lath-like IMCs were found in the interior of α-Al grains of the weld. An EDS analysis of the black lath-like

phase in Figure 9e was performed and the data showed that the lath-like IMC was also an Al_3Zr particle. Combined with the microstructure evolution (Figure 9) and the results of the mechanical properties including the tensile strength and microhardness (Figure 10) of the welded joints, it can be concluded that there is an optimum addition for element Zr. Adding excessive Zr element caused the segregation of the Zr atom in the weld, leading to the formation of large Al_3Zr IMCs and deteriorating the refining effect. In addition, Abdel-Hamid and Zaid [29] had revealed that when Zr and Ti elements existed simultaneously in the aluminum alloy and the content of Zr was more than the peritectic point, the excess Zr element could react with the original Al_3Ti particles and form large $Al_3(Ti_xZr_{1-x})$ IMCs, which resulted in the poisoning of Ti modification, and seriously deteriorated the microstructure and the mechanical properties of the welded joint. The above mechanism analysis can be used for explaining the fact that the tensile strength of the welded joint welded using Al-5Mg-0.5Zr wire was even lower than that of the welded joint welded using Zr-free wire. Due to the grain refinement strengthening mechanism owing to the addition of Zr element, the change trend of the elongation of the welded joint was in good agreement with that of the tensile strength of the welded joint.

3.5.1. Cast and Helix of Wire Electrode on a Spool

With regard to the Al-5Mg-0.12Zr wire electrode designed for high-speed automatic GMAW, the wire feedability of the wire electrode is dependent not only on the strength, hardness, roughness of the wire, but also on the winding state of the wire, which can be characterized by cast and helix of wire electrode on a spool. The most commonly used packaging of GMAW wire electrodes is the spool with an outside diameter of 300 mm. As shown in Figure 11, a sample of wire electrode should be taken from the spool large enough to form a loop when it is cut from the package, and then left unrestrained on the floor. Cast is essentially the diameter of the loop while helix is the rise of the wire electrode off of a flat surface. According to the winding requirements for GMAW solid wire electrodes specified by the American Welding Society (AWS), the cast should be not less than 381 mm and the helix should be less than 25 mm at any location [30].

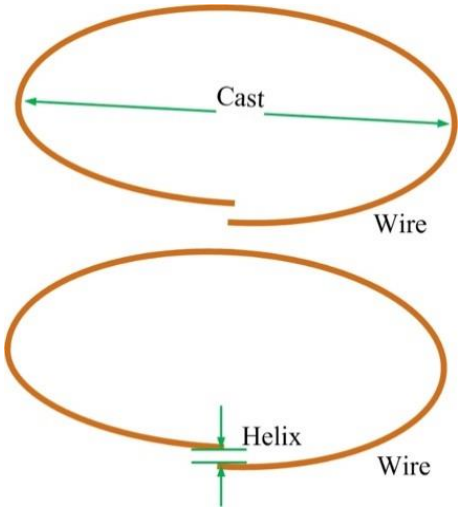

Figure 11. Cast and helix in a gas metal arc welding (GMAW) wire electrode.

3.5.2. Principle of the Novel Adjustable Apparatus

Figure 12 shows the plastic deformation of the wire electrode during drawing. As can be seen, drawing operations involve pulling wire through a die by means of a tensile force applied to the exit side of the die and the plastic flow is caused by compression force, arising from the reaction of the wire with the die. The last drawing die which causes the wire to produce plastic deformation can be defined as the exit die. As shown in Figure 13, there are two characteristic angles between an exit die and a pulling capstan. According to the literature [11], angle α in vertical plane affects the cast of the wire, angle β in horizontal plane affects the helix of the wire. When the angle α becomes small or

large, the corresponding curvature ρ of the wire will become large or small, leading to a corresponding decrease or increase in the cast of the wire. When the angle α is too small, a shape of "∞" would be found in the wire electrode unrestrained on the floor. The cause of the helix is the residual stress of the wire, which is induced by the uneven load on the wire during drawing. As shown in Figure 13b, angle β is equal to 90° when the wire is under balanced load conditions. While when the angle β is smaller than or greater than 90°, uneven load produces uneven plastic deformation in the wire, which leads the drawn wire to present a left-hand or right-hand spring-like shape.

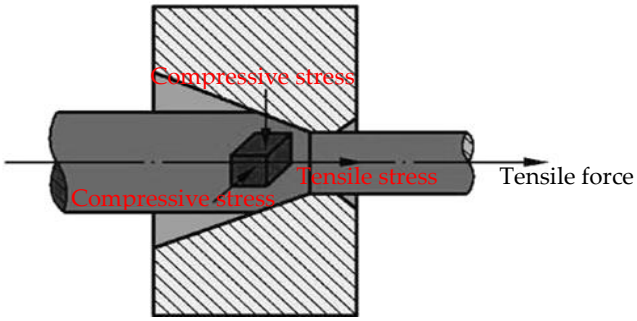

Figure 12. Schematic representation of drawing deformation process of wire electrode.

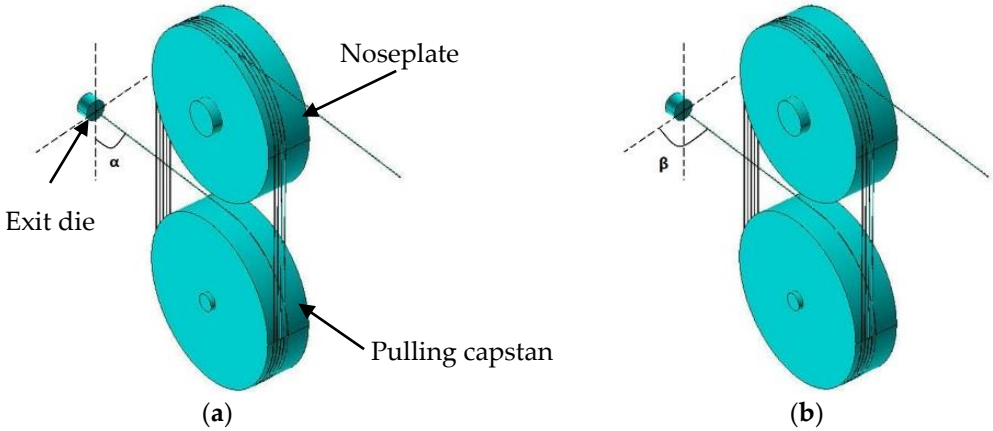

Figure 13. Schematic illustration of characteristic angles between an exit die and a pulling capstan: (**a**) angle α in the vertical plane; (**b**) angle β in the horizontal plane.

3.5.3. Structure and Application of the Novel Adjustable Apparatus

In practice, without considering the quality factor of the exit die itself, the helix is caused by the poor alignment of the exit die with capstan. Figures 14 and 15 show the physical picture and the schematic diagram of the novel apparatus for adjusting the cast and helix of the wire electrode, respectively. As shown in Figure 15a, part No. 1 is well located on the external wall of a finish drawing machine. Install part No. 2, 3, 4 in sequence after the installation of part No. 1 is completed. Then the core part No. 5 (Figure 15b) through the center holes of parts No. 1–4 is fixed with four screws. The exit die is placed into the part No. 5.

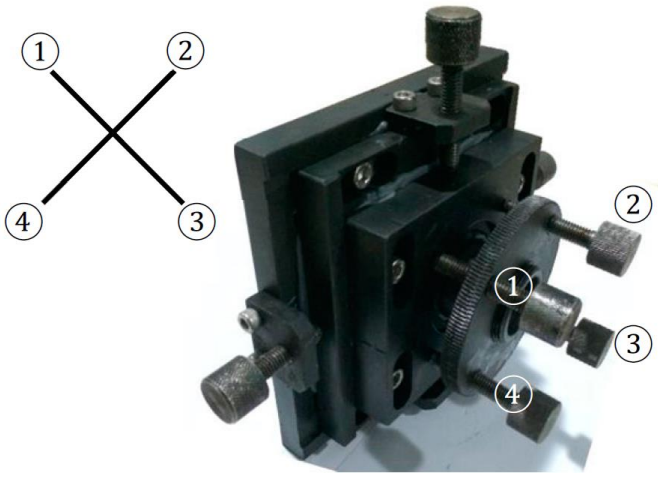

Figure 14. Physical picture of the novel apparatus for adjusting the cast and helix of wire electrodes.

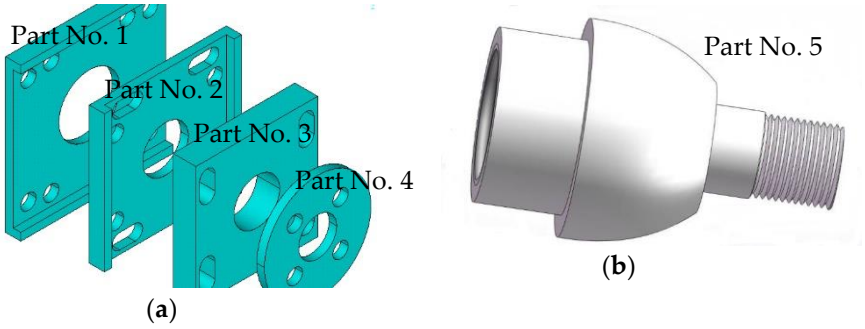

Figure 15. Schematic diagram of the novel apparatus: (**a**) basic parts of the apparatus; (**b**) core part of the apparatus.

According to the structure and principle of the apparatus, the rough adjustment of angle β can be achieved by the horizontal sliding of part No. 2 in the slideway of part No. 1, and the rough adjustment of angle α can be achieved by the vertical sliding of part No. 3 in the slideway of part No. 2. The fine adjustments of angle α and β are mainly achieved by the slack level of threaded connection of the four screws, which are numbered as ①–④ in a clockwise order (Figure 14).

The results of the adjustment of the Al-5Mg-0.12Zr wire electrode cast are shown in Figure 16, and the cast increased gradually during the adjustment of angle α, which was performed by keeping the adjustment of ① synchronized with that of ②, and the adjustment of ③ synchronized with that of ④. Figure 17 shows the adjustment results of helix. Keep the adjustment of ① synchronized with that of ④, and keep the adjustment of ② synchronized with that of ③. When the screw-in depth of ① and ④ was much smaller than that of ② and ③, the angle β was far less than 90°, the wire showed a left-hand spring-like structure and the helix was large in value (Figure 17a). By further increasing the screw-in depth of ① and ④ and decreasing that of ② and ③ at the same time, the left hand helix was reduced to 65 mm, but the value was still unqualified (Figure 17b), which still meant the angle $\beta < 90°$. When the angle β was adjusted to 90° by changing the screw-in depths of ①–④ to some extent, the helix of the wire was 0 mm (Figure 17c), which met the AWS requirements for wire feedability. However, further increasing the screw-in depth of ① and ④ on the basis of 0 mm helix, the wire began to show a right-hand structure and the helix was increased again (Figure 17d), which meant the angle $\beta > 90°$. It can be concluded from the results of adjustment of the wire (Figures 16 and 17) that the apparatus can effectively adjust the cast and helix of the wire and lead the wire to satisfy the AWS requirements for wire feedability.

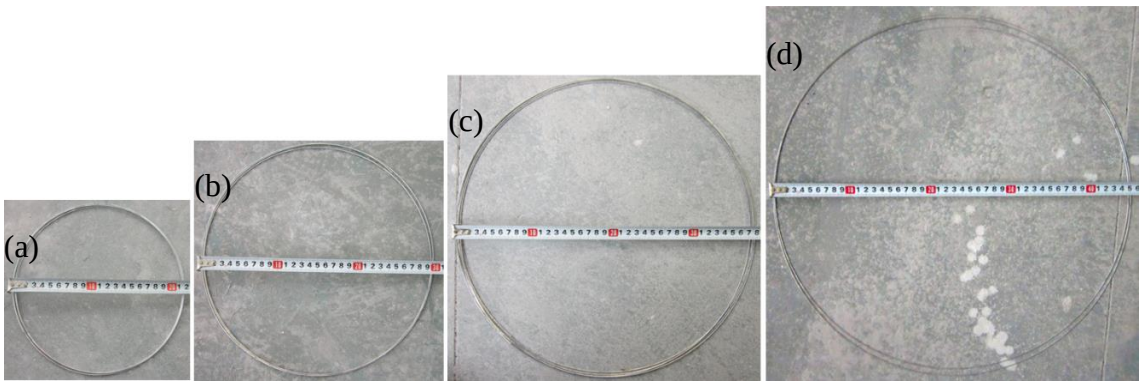

Figure 16. Measured values of cast during adjusting process: (**a**) cast = 215 mm; (**b**) cast = 295 mm; (**c**) cast = 375 mm; (**d**) cast = 450 mm.

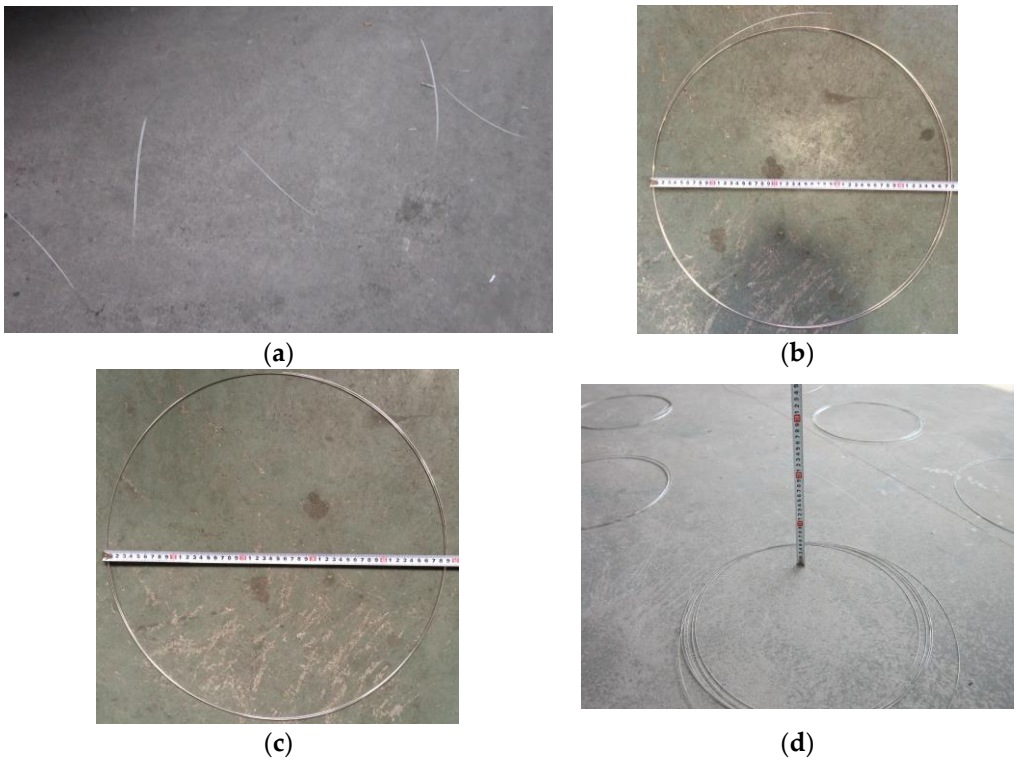

Figure 17. Measured values of helix during adjusting process: (**a**) left hand, helix = ∞; (**b**) left hand, helix = 65 mm; (**c**) helix = 0 mm; (**d**) right hand, helix = 215 mm.

4. Conclusions

The effect of Zr on the microstructure and mechanical properties of Al-5Mg wire alloys and the resulting welded joints was investigated. In addition, factors that affect the wire feedability of the wire electrodes were also analyzed, and a novel adjustable apparatus was introduced and discussed. The conclusions are as follows.

(1) The addition of 0.12 wt % Zr could refine α-Al dendrites of the as-cast Al-5Mg wire alloy due to the increased amount of heterogeneous substrates for nucleation of α-Al grains, while an excess addition of Zr could result in the coarsening of the α-Al dendrites.

(2) The tensile strength, microhardness, and surface roughness of 1.2 mm Al-5Mg wire electrodes, as well as the tensile strength and elongation of the resulting welded joints, were improved by adding an appropriate amount of Zr, which indicated that Zr addition could improve not only the mechanical properties of welded joints, but also the wire feedability of the Al-5Mg wire electrode bearing Zr.

(3) The cast and helix of wire electrode are two key indices for wire feedability of the Al-5Mg wire electrode, which are affected by the two characteristic angles α and β between the exit die and the pulling capstan. The novel apparatus, which consisted of five parts and four screws, could achieve the rough and fine adjustments of the angle α and β, producing a perfect alignment of exit die with capstan to ensure consistency in wire characteristics.

Acknowledgments: This work is financially supported by the National Natural Science Foundation of China (Grant No. 51375233, 51305173), China Postdoctoral Science Foundation (General Financial Grant No. 2014M550289, Special Financial Grant No. 2015T80548), and the Priority Academic Program Development of Jiangsu Higher Education Institutions (PAPD).

Author Contributions: Bo Wang, Songbai Xue and Jianxin Wang conceived and designed the experiments; Bo Wang and Chaoli Ma performed the experiments; Bo Wang and Songbai Xue analyzed the data; Zhongqiang Lin contributed reagents/materials/analysis tools; Bo Wang wrote the paper.

Conflicts of Interest: The authors declare no conflict of interest.

References

1. De Filippis, L.A.C.; Serio, L.M.; Facchini, F.; Mummolo, G.; Ludovico, A.A. Prediction of the vickers microhardness and ultimate tensile strength of AA5754 H111 friction stir welding butt joints using artificial neural network. *Materials* **2016**, *9*, 915, doi:10.3390/ma9110915.
2. Haddag, B.; Atlati, S.; Nouari, M.; Moufki, A. Dry machining aeronautical aluminum alloy AA2024-T351: analysis of cutting forces, chip segmentation and built-up edge formation. *Metals* **2016**, *6*, 197, doi:10.3390/met6090197.
3. Shen, L.; Chen, H.; Che, X.L.; Xu, L.D. Corrosion–fatigue crack propagation of aluminum alloys for high-speed trains. *Int. J. Mod. Phys. B* **2017**, *31*, 1744009, doi:10.1142/s021797921744009x.
4. Kee Paik, J.; Thayamballi, A.K.; Sung Kim, G. The strength characteristics of aluminum honeycomb sandwich panels. *Thin-Walled Struct.* **1999**, *35*, 205–231.
5. Balasubramanian, V.; Ravisankar, V.; Madhusudhan Reddy, G. Effect of pulsed current welding on mechanical properties of high strength aluminum alloy. *Int. J. Adv. Manuf. Technol.* **2008**, *36*, 254–262.
6. Kalemba-Rec, I.; Hamilton, C.; Kopyściański, M.; Miara, D.; Krasnowski, K. Microstructure and mechanical properties of friction stir welded 5083 and 7075 aluminum alloys. *J. Mater. Eng. Perform.* **2017**, *26*, 1032–1043.
7. Wang, B.; Xue, S.B.; Ma, C.L.; Wang, J.X.; Lin, Z.Q. Effects of porosity, heat input and post-weld heat treatment on the microstructure and mechanical properties of TIG welded joints of AA6082-T6. *Metals* **2017**, *7*, 463.
8. Enz, J.; Riekehr, S.; Ventzke, V.; Huber, N.; Kashaev, N. Fibre laser welding of high-alloyed Al-Zn-Mg-Cu alloys. *J. Mater. Process. Technol.* **2016**, *237*, 155–162.
9. Tang, L.X.; Huang, X.X.; Li, Y.F.; Wang, X.J. Shallow of aluminum and aluminum alloy MIG welding wire feed stability influence factors. *Weld. Appl.* **2015**, *7*, 41–43.
10. Padilla, T.M.; Quinn, T.P.; Munoz, D.R.; Rorrer, R.A.L. A mathematical model of wire feeding mechanisms in GMAW. *Weld. J.* **2003**, *82*, 100–109.
11. Xu, R.H. Control of pitch and relaxation diameter in welding wire production. *Met. Prod.* **2013**, *39*, 6–7.
12. Anderson, B.E. Lubricated Aluminum Weld Wire and Process for Spooling It. U.S. Patent 4,913,927, 3 April 1990. Available online: http://www.freepatentsonline.com/4913927.pdf (accessed on 21 September 2017).
13. Aluminum GMAW-Gas Metal Arc Welding for Aluminum Guide. Available online: http://www.lincolnelectric.com/assets/global/Products/Consumable_AluminumMIGGMAWWires-SuperGlaze-SuperGlaze5356TM/c8100.pdf (accessed on 22 September 2017).
14. AlcoTec Aluminum Technical Guide. Available online: http://www.esabna.com/shared/documents/litdownloads/alc-10029b_alcotec_technical_guide.pdf (accessed on 22 September 2017).
15. Belov, N.A.; Alabin, A.N.; Matveeva, I.A.; Eskin, D.G. Effect of Zr additions and annealing temperature on electrical conductivity and hardness of hot rolled Al sheets. *Trans. Nonferr. Met. Soc.* **2015**, *25*, 2817–2826.
16. Chao, R.Z.; Guan, X.H.; Guan, R.G.; Tie, D.; Lian, C.; Wang, X.; Zhang, J. Effect of Zr and Sc on mechanical properties and electrical conductivities of Al wires. *Trans. Nonferr. Met. Soc.* **2014**, *24*, 3164–3169.

17. Shen, Y.F.; Guan, R.G.; Zhao, Z.Y.; Misra, R.D.K. Ultrafine-grained Al-0.2Sc-0.1Zr alloy: The mechanistic contribution of nano-sized precipitates on grain refinement during the novel process of accumulative continuous extrusion. *Acta Mater.* **2015**, *100*, 247–255.
18. Xu, Z.; Zhao, Z.H.; Wang, G.S.; Zhang, C.; Cui, J.Z. Microstructure and mechanical properties of the welding joint filled with microalloying 5183 aluminum welding wires. *Int. J. Miner. Metall. Mater.* **2014**, *21*, 577–582.
19. Zhang, Z.H.; Dong, S.Y.; Wang, Y.J.; Xu, B.S.; Fang, J.X.; He, P. Microstructure characteristics of thick aluminum alloy plate joints welded by fiber laser. *Mater. Des.* **2015**, *84*, 173–177.
20. Taendl, J.; Orthacker, A.; Amenitsch, H.; Kothleitner, G.; Poletti, C. Influence of the degree of scandium supersaturation on the precipitation kinetics of rapidly solidified Al-Mg-Sc-Zr alloys. *Acta Mater.* **2016**, *117*, 43–50.
21. Norman, A.F.; Birley, S.S.; Prangnell, P.B. Development of new high strength Al-Sc filler wires for fusion welding 7000 series aluminium aerospace alloys. *Sci. Technol. Weld. Join.* **2003**, *8*, 235–245.
22. BS EN 14532–3:2004(E), Welding Consumables-Test Methods and Quality Requirements-Part 3: Conformity Assessment of Wire Electrodes, Wires and Rods for Welding of Aluminum Alloys. Available online: http://www.anystandards.com/plus/download.php?open=0&aid=4926&cid=3 (accessed on 11 September 2017).
23. Ma, C.G.; Qi, S.Y.; Li, S.; Xu, H.Y.; He, X.L. Melting purification process and refining effect of 5083 Al-Mg alloy. *Trans. Nonferr. Metal. Soc.* **2014**, *24*, 1346–1351.
24. Grimes, R.; Dashwood, R.J.; Harrison, A.W.; Flower, H.M. Development of a high strain rate superplastic Al-Mg-Zr alloy. *Mater. Sci. Technol.* **2000**, *16*, 1334–1339.
25. Ocenasek, V.; Slamova, M. Resistance to recrystallization due to Sc and Zr addition to Al-Mg alloys. *Mater. Charact.* **2001**, *47*, 157–162.
26. Schempp, P.; Cross, C.E.; Pittner, A.; Oder, G.; Neumann, R.S.; Rooch, H.; Dörfel, I.; Österle, W.; Rethmeier, M. Solidification of GTA aluminum weld metal: Part I—Grain morphology dependent upon alloy composition and grain refiner content. *Weld. J.* **2014**, *93*, 53–59.
27. Yang, D.X.; Li, X.Y.; He, D.Y.; Huang, H. Effect of minor Er and Zr on microstructure and mechanical properties of Al-Mg-Mn alloy (5083) welded joints. *Mater. Sci. Eng. A* **2013**, *561*, 226–231.
28. Knipling, K.E.; Dunand, D.C.; Seidman, D.N. Precipitation evolution in Al-Zr and Al-Zr-Ti alloys during aging at 450–600 °C. *Acta Mater.* **2008**, *56*, 1182–1195.
29. Abdel-Hamid, A.A.; Zaid, A.I.O. Poisoning of grain refinement of some aluminium alloys. In Proceedings of the Current Advances in Mechanical Design and Production, Seventh Cairo University International MDP Conference, Cairo, Egypt, 15–17 February 2000; pp. 331–338.
30. Gas Metal Arc Welding. Available online: https://www.lincolnelectric.com/assets/global/products/consumable_miggmawwires-superarc-superarcl-56/c4200.pdf (accessed on 15 September 2017).